Nonstationary signal analysis of magnetic islands in plasmas

E. D. Taylor,[a] C. Cates, M. E. Mauel, D. A. Maurer, D. Nadle, G. A. Navratil, and M. Shilov
Department of Applied Physics and Applied Mathematics, Columbia University, New York, New York 10027

(Received 14 May 1999; accepted for publication 10 September 1999)

Rotating magnetic islands produce fluctuations on a variety of diagnostics in magnetic fusion energy plasmas. The analysis of these fluctuations requires the calculation of the amplitude, phase, and frequency of the oscillations. These three spectral quantities generally evolve in time, necessitating nonstationary signal analysis techniques. The Hilbert transform offers an efficient and accurate method of calculating these three quantities from one diagnostic signal. This feature allows the Hilbert transform to determine the success of the active rotation control of magnetic islands, and to calculate the profile of the diagnostic measurements in a frame of reference co-rotating with the magnetic island. Comparisons to quadrature and spectrogram techniques demonstrate the accuracy of the Hilbert transform method. © *1999 American Institute of Physics.* [S0034-6748(99)04812-1]

I. INTRODUCTION

Magnetic islands are common in a wide variety of magnetic fusion energy (MFE) devices.[1] Magnetic islands generally rotate in these devices, creating perturbations that appear on diagnostics as a signal

$$f(t)=a(t)\cos[\varphi(t)], \tag{1}$$

where $a(t)$ is the amplitude of the perturbation and $\varphi(t)$ is the phase. Figure 1 plots a typical signal, along with the amplitude, frequency, and phase of the signal. The time evolution of the amplitude and frequency makes the calculation of the spectral quantities difficult. Standard analysis methods using discrete Fourier transforms[2] fail because of the time evolution, necessitating nonstationary signal analysis techniques in order to capture the island dynamics. The Hilbert transform offers an efficient and straightforward technique for calculating the time evolution of the amplitude, phase, and frequency of magnetic island perturbations. The Hilbert transform is extensively used in signal processing applications to determine the spectral quantities of signals from a variety of sources.[3–5] The use of this transform in plasma physics has been largely limited to theoretical work. The Hilbert transform calculated the complex envelope of high frequency electromagnetic waves in plasmas in order to reduce the computational time and ease the comparison with theory.[6] Another application calculated the Hilbert transform of a Gaussian function to produce the dispersion function, $Z(\xi)$, for waves in hot plasmas.[7] However, the application to magnetic island studies has been limited.

An importance focus of current magnetic fusion research is the control of magnetic islands with resonant magnetic perturbations (RMPs). These perturbations mimic the magnetic structure of the islands, providing an external means for interacting with the island. Synchronous RMPs act to reduce the island size through negative feedback, using the magnetic perturbation from the island as the input signal.[8–10] Measurements of the island phase $\varphi(t)$ determine the proper perturbation phase for producing negative feedback. Changes in the magnetic island amplitude $a(t)$ and the rotation frequency $\nu(t)$ measure the success of the feedback control. Asynchronous RMPs attempt to reduce the island size by changing the rotation frequency of the magnetic island.[8–10] Theories predict that changes in the interaction between the magnetic island and the plasma will reduce the island amplitude.[11] Measurements of the island amplitude $a(t)$ and frequency $\nu(t)$ also judge the success of rotation control. Furthermore, since the success of the damping depends on the interaction with the plasma, the spectral response of plasma perturbations to rotation control also requires measurement. Finally, fundamental studies of island behavior focus on how the magnetic island structure interacts with the plasma.[12,13] Since this structure rotates in experiments, diagnostics measure the island properties in the laboratory frame rather than the magnetic island frame of reference. Knowledge of the measurement phase allows the conversion to a frame of reference co-rotating with the island, providing data that can be more directly compared to theoretical predictions.

The importance of the amplitude, phase, and frequency in magnetic island studies led to the implementation of a wide range of techniques to determine these spectral quantities. The simplest technique tracks the maximum and minimum of magnetic signals to determine the location of the magnetic O and X points, respectively, of the magnetic island.[14,15] A similar method tracks the zero crossing of the magnetic signals from spatially separated detectors to quantify the island propagation.[16] The main weakness of these methods is that they ignore the bulk of the data at the expense of only one or two points per cycle. Meaningful analysis requires lengthy time sampling with slow changes in the amplitude and frequency. The quadrature technique can also measure the spectral quantities of magnetic islands.[9] However, this technique can only analyze signals that possess both a sine and cosine phase, limiting its application. Spectrogram analysis calculates the time history of the full Fou-

[a]Present address: Cutler-Hammer, Vacuum Interrupter Technology Dept., Horseheads, NY 14845; electronic mail: tayloed@ch.etn.com.

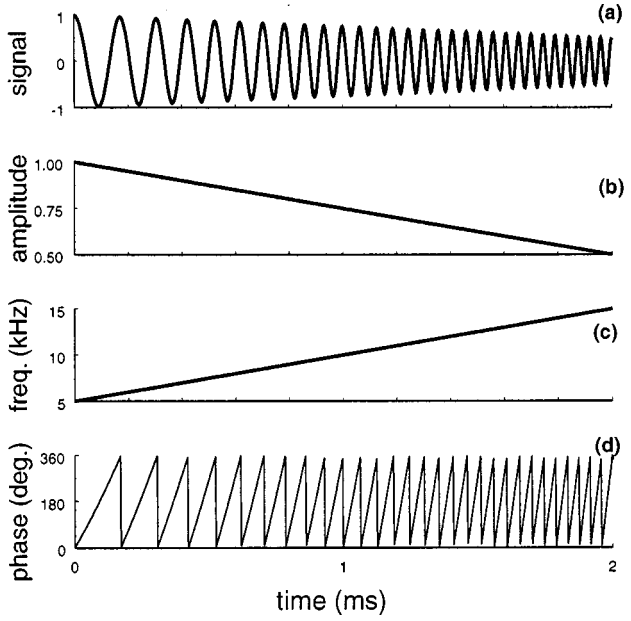

FIG. 1. Example of a nonstationary signal. (a) Signal $a(t)\cos[\varphi(t)]$, (b) amplitude $a(t)$, (c) frequency $\nu(t)$, and (d) phase $\varphi(t)$.

rier spectrum of island signals.[15,17] The spectrogram generally wastes the bulk of the performed calculations for island studies, since normally the evolution of only one frequency component is of interest. The complex demodulation heterodyne technique reduces the number of calculations compared to the spectrogram, but retains information on the fundamental frequency and the harmonics of the island perturbation.[18] However, the method requires additional programming and the careful selection of a digital filter. The key advantage of the Hilbert transform method is that it offers a straightforward and efficient method for calculating the three spectral quantities from one signal. In addition, the transform is already implemented in many data analysis programs, such as IDL[19] and MATLAB,[20] allowing the straightforward application to magnetic island data.

II. HILBERT TRANSFORM

This section summarizes the Hilbert transform properties relevant to magnetic island measurements. Determining the spectral quantities is simple if the quadrature component of the signal is known.[21,22] A quadrature signal is 90° out of phase with respect to the original signal. The quadrature component for Eq. (1) is

$$g(t)=a(t)\sin[\varphi(t)]. \tag{2}$$

The combination of Eqs. (1) and (2) can determine the amplitude, phase, and frequency of the signal using the respective relations

$$a(t)=\sqrt{f^2(t)+g^2(t)}, \tag{3}$$

$$\varphi(t)=\tan^{-1}\left(\frac{g(t)}{f(t)}\right), \tag{4}$$

$$\nu(t)=\frac{1}{2\pi}\frac{d\varphi}{dt}=\frac{1}{2\pi}\frac{(dg/dt)f-(df/dt)g}{f^2+g^2}. \tag{5}$$

Equations (1) and (2) can be combined to form the analytic function $s(t)$[4,21,22]

$$\begin{aligned} s(t)&=a(t)e^{i\varphi(t)}\\ &=a(t)\{\cos[\varphi(t)]+i\sin[\varphi(t)]\}\\ &=f(t)+ig(t). \end{aligned} \tag{6}$$

Using the analytic function, Eqs. (3)–(5) can determine the spectral quantities by taking the real and imaginary parts of $s(t)$ to get $f(t)$ and $g(t)$.

The Hilbert transform $H\{f(t)\}$ approximates the analytic function using only one input signal. The function is defined as[4]

$$H\{f(t)\}=f(t)+i\int_{-\infty}^{\infty}\frac{f(t-\tau)}{\pi\tau}d\tau. \tag{7}$$

Unfortunately, multiple ways of analytically and numerically defining the Hilbert transform exist. This analytic definition differs from some formulas[21,22] by the addition of the $f(t)$ term in order to make the function definition equivalent to the numerical implementation in MATLAB.[20] The transform is calculated numerically using fast Fourier transforms (FFT). The FFT of the signal is calculated, then the amplitude of all the negative frequencies are set to zero. This modified FFT is then inverted to produce the Hilbert transform. The output of this Hilbert transform method approximates the analytic signal

$$H\{f(t)\}=s(t)=a(t)e^{i\varphi(t)}. \tag{8}$$

Other numerical implementations of the Hilbert transform exist. One example is in IDL,[19] where for the default option the entire FFT transform is multiplied by the imaginary number i and then inverted. The output of this method is the negative of the quadrature signal, $-a(t)\sin[\varphi(t)]$, rather than the analytic signal directly. The only significant difference between these and other methods is the exact process necessary to convert the Hilbert transform output into the quadrature signal. Once this process is determined, the different Hilbert transform methods are equivalent.

Two issues in the use of the Hilbert transform are the uniqueness of the output and how closely $H\{f(t)\}$ approximates the analytic signal $s(t)$.[21] The attempt to use one signal, the diagnostic data, to derive two signals, the amplitude and phase, creates the uniqueness problem. Changes in the oscillation behavior of $f(t)$ can be attributed to changes in either $a(t)$ or $\cos[\varphi(t)]$. The Hilbert transform overcomes this difficulty by providing a well-defined algorithm for deriving two functions, $f(t)$ and $g(t)$, from the signal data. These two functions can then derive two more unique functions, the amplitude and phase, using Eqs. (3) and (4). Thus, the Hilbert transform will always produce a unique answer. This shifts the problem to whether the amplitude and phase behavior calculated with the two unique functions is meaningful.

Two conditions determine the accuracy of approximating the analytic signal with the Hilbert transform. These conditions place experimental requirements on the process being measured. The first condition stems from the ambiguity

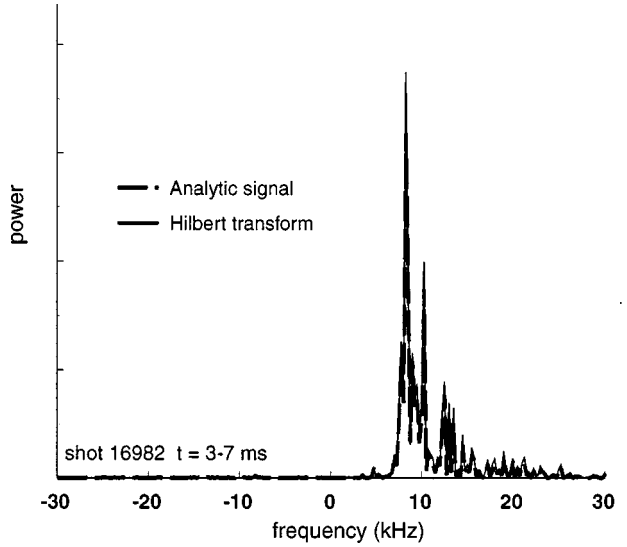

FIG. 2. Comparison of the power spectrums of the Hilbert transform of the cosine signal from a $m=2$ detector and the analytic signal constructed with the cosine and sine signals.

about whether observed oscillations reflect changes in the amplitude or in the frequency. For the signal,

$$f(t)=\cos(2\pi\nu_1 t)\cos(2\pi\nu_2 t), \quad \text{where} \quad \nu_2>\nu_1, \tag{9}$$

the phase could be defined as $\varphi(t)=2\pi\nu_2 t$ with the amplitude variation as $a(t)=\cos(2\pi\nu_1 t)$, or vice versa. The Hilbert transform overcomes this difficulty by selecting the higher frequency for the phase evolution.[4,21] Hence, the application of the Hilbert transform to Eq. (9) produces

$$H\{f(t)\}=\cos(2\pi\nu_1 t)e^{i(2\pi\nu_2 t)}. \tag{10}$$

Thus, the amplitude variation in the signal must be slower than the island motion frequency. The second experimental condition states that the spectra of $a(t)$ and $\cos[\varphi(t)]$ must be separated in frequency.[21] Application of the Hilbert transform would place the slower variation into the amplitude and the faster into the phase, thereby mixing the two changes together and degrade the accuracy the calculated spectral quantities.

Magnetic islands generally meet these two conditions. The $m=2/n=1$ islands on the HBT-EP (High Beta Tokamak - Extended Pulse) tokamak rotate with a frequency in the range of $\nu\approx 5-15$ kHz and an amplitude evolution of $\leqslant 2$ kHz for both naturally rotating and externally controlled islands.[9] These islands meet the condition that the amplitude variation is slower than the rotation frequency, and that the two spectra are separated in frequency.

Fourier analyzing $m=2$ coils offer the opportunity to compare the Hilbert transform output to the actual analytic function. These coils detect the $m=2$ magnetic island and possess both a sine and cosine phase. The two signals can construct the analytic signal $s(t)$

$$s(t)=f_{\cos}(t)+ig_{\sin}(t), \tag{11}$$

where $f_{\cos}(t)$ is the cosine phase output and $g_{\sin}(t)$ is the sine phase output. Figure 2 compares the energy spectrum of $s(t)$ to the energy spectrum of the Hilbert transform of the cosine phase, $H\{f_{\cos}(t)\}$. The energy for both functions is concentrated in the positive frequency portion of the spectrum. The close agreement between the spectrums indicates that the Hilbert transform reproduces the analytic function. Since this implementation of the Hilbert transform sets the negative frequencies to zero, the lack of significant power levels at negative frequencies for the actual analytic function suggests that the Hilbert transform method accurately calculates this function.

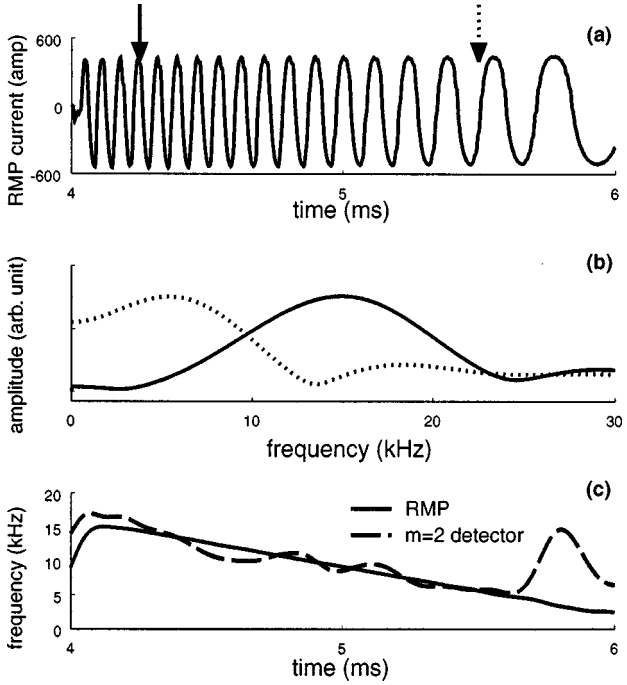

FIG. 3. Rotation control experiment. (a) Applied RMP, (b) frequency spectrum for data windowed around the points indicated by the arrows in (a). (c) Plots the frequency $\nu(t)$ for the RMP and the magnetic island.

The main exception to these conditions occurs during the locking of magnetic islands to stationary perturbations. Here, the island motion stops, bringing the frequency to zero. This slowing generally couples to a rapid growth in the island size.[23,24] The slowing of the island rotation and the increasing rate of island growth will eventually bring the frequency of rotation near that of the amplitude variation, violating the second condition. As the island motion ceases, the first condition will be violated. Nevertheless, rotation experiments focusing on changing the rotation frequency rather than locking the island motion will generally meet these conditions.

III. APPLICATIONS

Rotation control experiments on $m=2/n=1$ magnetic islands in HBT-EP[8,9] demonstrate the utility of the Hilbert transform. Resonant magnetic perturbations (RMPs) control the island rotation by resonantly interacting with the magnetic structure of the island. Changing the frequency of the perturbation changes the island rotation frequency. Figure 3 illustrates a typical RMP, where the frequency is ramped down from 15 to 2 kHz, decelerating the island. An important issue in these experiments is the success of the RMP in changing the island motion. Indications of success appear in the frequency analysis of the magnetic island behavior. The magnetic perturbation from the island was windowed over

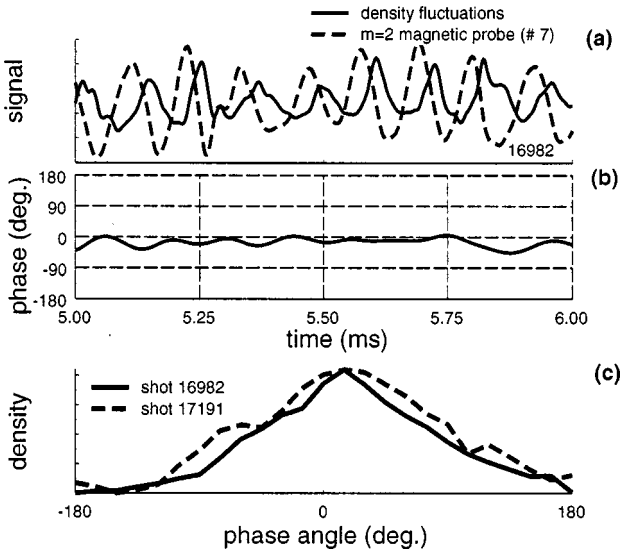

FIG. 4. Phase calculations for magnetic and density perturbations. (a) Plots the actual signals. (b) Plots the phase difference, accounting for the detector locations. (c) Plots the density as a function of island phase for two different shots.

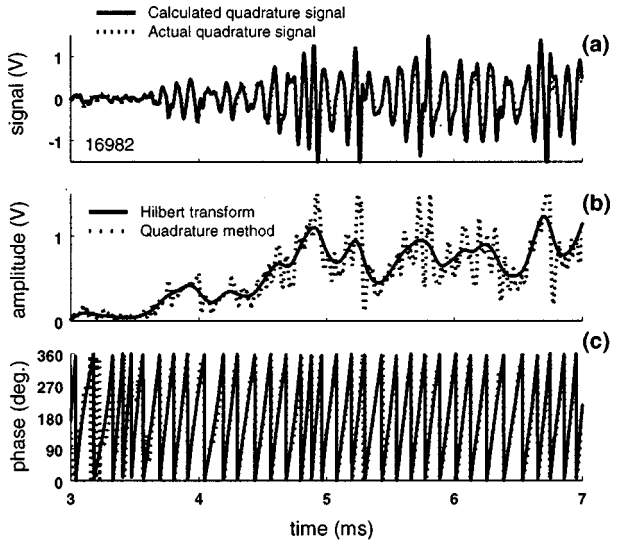

FIG. 5. Comparison of quadrature and Hilbert calculations of the (a) quadrature signal, (b) frequency, and (c) phase.

two small time intervals, one early and one late in the ramp [Fig. 3(b)], then fast Fourier transformed. The motion of the peak frequency demonstrates that the RMP changed the island frequency. However, the most useful plot would directly compare the time evolution of the island frequency to that of the RMP. The Hilbert transform calculates this information in Fig. 3(c), illustrating the extent to which the RMP changes the island rotation. Because changes in the island rotation depend on a variety of plasma effects, this information is crucial to analyzing these experiments.

A second application of the Hilbert transform compares the phase information of magnetic island data taken by diagnostics at different locations and/or measuring different properties. The phase difference between the diagnostic and the magnetic signal determines the location of the diagnostic measurement within the rotating magnetic island structure. This effectively moves the signal into a frame of reference corotating with the island. For example, a phase from the poloidal field measurement of zero could correspond to the magnetic *O* point of the island, while a phase of $\pm\pi$ would in turn correspond to the *X* point. One application determines the location of perturbations in the density within the island structure as measured by a microwave interferometer (Fig. 4). The lack of a quadrature signal for the interferometer, combined with the separate locations of the interferometer and magnetic diagnostics, makes direct interpretation of the phase difference between the perturbations difficult. The Hilbert transform straightforwardly calculates the phase of the interferometer and magnetic coil measurements. Removing the phase shift due to the different positions of these diagnostics determines the time-resolved phase difference [Fig. 4(b)]. This phase difference is approximately zero, indicating that the density peaks occur in phase with increases in the poloidal magnetic field. This determines that the density is peaked near the island *O* point.

This analysis can be extended to determining the behavior of a diagnostic signal in terms of the magnetic island structure. This application builds on the previous example. Rather than simply determining that the peak in the density occurs at the peak in the poloidal field, the entire density profile across the island can be calculated using the phase. The phase of the magnetic signal determines the location within the island of the measurement. Taking the phase of the magnetic signal, accounting for the phase shift due to the diagnostic positions, and then averaging over a small time interval produces a picture of the diagnostic measurement in terms of the phase of the magnetic signal [Fig. 4(c)]. This allows for the study of the changes in the island structure across different discharge types, or for different diagnostic setups, such as different positions of Langmuir probes.

IV. COMPARISON TO OTHER METHODS

The presence of a cosine and sine phase of the $m=2$ coils allows the direct comparison of the Hilbert transform to exact quadrature calculations. The quadrature function $g(t)$ generated by the Hilbert transform [Eq. (6)] can be directly compared to the actual quadrature signal $g_{\sin}(t)$ [Eq. (11)] from the sine coil [Fig. 5(a)]. The amplitude and phase from these two methods is compared in Figs. 5(b) and 5(c). The Hilbert transform closely reproduces the actual quadrature function. The amplitude and phase calculated with the Hilbert transform in turn closely match the actual quadrature data. The key advantage of the Hilbert transform method is that only one signal is required to generate the amplitude and phase. The method is well suited for diagnostics lacking a quadrature signal, such as Langmuir probes, soft x-ray detectors, and density measurements.

A common method used to determine the frequency and amplitude when no quadrature signal is present is the spectrogram, also known as the time-frequency distribution.[3] A moving window generates the time-resolved frequency and relative amplitude, producing full frequency spectrum at each time point. Selecting the peak amplitude at each time point determines the time behavior of the dominant fre-

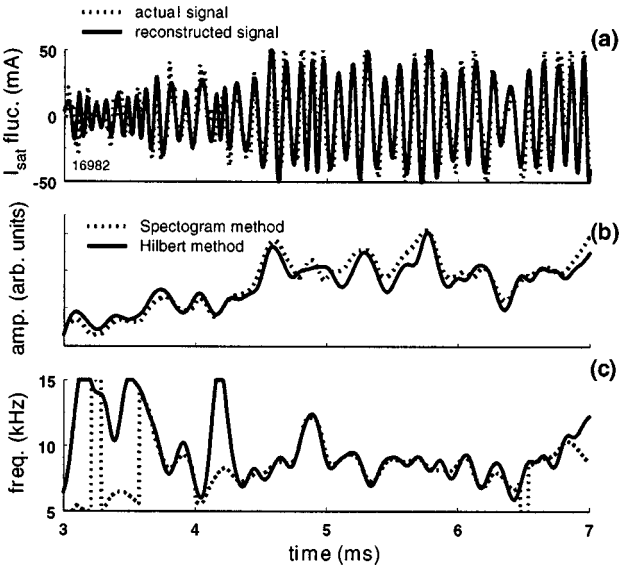

FIG. 6. Comparison of spectrogram and Hilbert calculations of the (a) signal, (b) amplitude, and (c) frequency.

quency and the relative amplitude. The application to ion saturation current measurements of island perturbations is plotted in Fig. 6. The amplitude and frequency demonstrate strong agreement between the two methods.

There are two advantages of the Hilbert transform method over the spectrogram. First, the Hilbert transform is a significantly faster algorithm. Table I compares the number of FFTs and floating point operations required by both algorithms to analyze the same data. Generating the spectrogram required 1000 times more FFTs and approximately 60 times more floating-point operations than the Hilbert transform for the equivalent calculations. This saving translates into a significant increase in speed. The second advantage of the Hilbert transform stems from the ability to calculate both the phase and an amplitude in the original signal units. Phase calculations using the spectrogram are unstable to small errors in the peak frequency. The small window required for high time resolution produces a large spread in the frequency domain, making selection of the peak frequency prone to small errors. However, the Hilbert transform can robustly calculate the phase in the presence of error, as discussed in the next section. This allows for the simple reconstruction of the original signal from the calculated amplitude $a(t)$ and phase $\varphi(t)$

$$f_r(t)=a(t)\cos[\varphi(t)]. \tag{12}$$

The reconstructed signal $f_r(t)$ can be directly compared to the original signal to determine the effect of the various filtering and smoothing operations [Fig. 6(a)]. Spectral techniques invariably require filtering and/or smoothing of the signal, and the net effect on the spectral results is generally difficult to determine. A direct comparison of the original and reconstructed signal quickly highlights these effects. Furthermore, the comparison can also determine whether the signal behaves in a nonsinusoidal fashion, helping to determine when and how spectral techniques fail to fully describe the signal behavior.

TABLE I. Comparison of the number of calculations required by Hilbert transform and spectrogram processing of the data in Fig. 1.

	Number of FFTs	Floating point operations
Hilbert transform	2	~15 000 000
Spectrogram	2001	~880 000 000

The main disadvantage of the Hilbert transform method compared to the spectrogram is that the Hilbert method requires the signal to have only one dominant component. Signals of the form

$$f(t)=a_1(t)\cos[\varphi_1(t)]+a_2(t)\cos[\varphi_2(t)]+\cdots, \tag{13}$$

where the amplitudes are on the same order of magnitude, $a_1 \sim a_2 \sim \ldots$, do not produce a meaningful amplitude and phase when calculated with the Hilbert transform, nor when calculated with quadrature techniques in general. Instead, the full spectrogram is required to individually trace the behavior of the various frequency components. When the diagnostic signal is dominated by oscillations from a single island structure, then the Hilbert transform may be generally used. More advanced techniques are required if the diagnostic signal contains information on multiple magnetic islands.

V. ERROR ANALYSIS

The Hilbert transform retains its ability to determine the amplitude and phase of a signal even in the presence of white noise and/or a lower amplitude signal component. The error due to white noise in the amplitude calculation is estimated by starting with the signal

$$f(t)=a(t)\cos[\varphi(t)]+\varepsilon_f(t), \tag{14}$$

where ε_f is the white noise in the signal. The quadrature component calculated with the Hilbert transform would be

$$\begin{aligned} g(t)&=\mathrm{Im}[H\{f(t)\}]=\mathrm{Im}(H\{a(t)\cos[\varphi(t)]\}+H\{\varepsilon_f(t)\}) \\ &=a(t)\sin[\varphi(t)]+\varepsilon_g(t), \\ \varepsilon_g&=\mathrm{Im}[H\{\varepsilon_f\}]. \end{aligned} \tag{15}$$

Since the Hilbert transform only alters the phase of a signal, ε_g is essentially ε_f with the frequency components shifted by ninety degrees. Because the phase of white noise is random, both ε_f and ε_g possess the same noise amplitude. Thus, the error due to noise of both the original signal and its quadrature component is the standard deviation of the noise

$$\sigma \approx \text{std dev}(\varepsilon_f) \approx \text{std dev}(\varepsilon_g). \tag{16}$$

Calculating the error in the amplitude σ_{amp} using the standard formula for the propagation of errors[25] gives

$$\begin{aligned} \sigma_{\text{amp}}&=\sqrt{\left(\frac{\partial a}{\partial f}\right)^2\sigma^2+\left(\frac{\partial a}{\partial g}\right)^2\sigma^2} \\ &=\left[\left(\frac{f}{\sqrt{f^2+g^2}}\right)^2+\left(\frac{g}{\sqrt{f^2+g^2}}\right)^2\right]^{1/2}\sigma=\sigma, \end{aligned} \tag{17}$$

where the error in the amplitude is equal to the white noise error in the original signal.

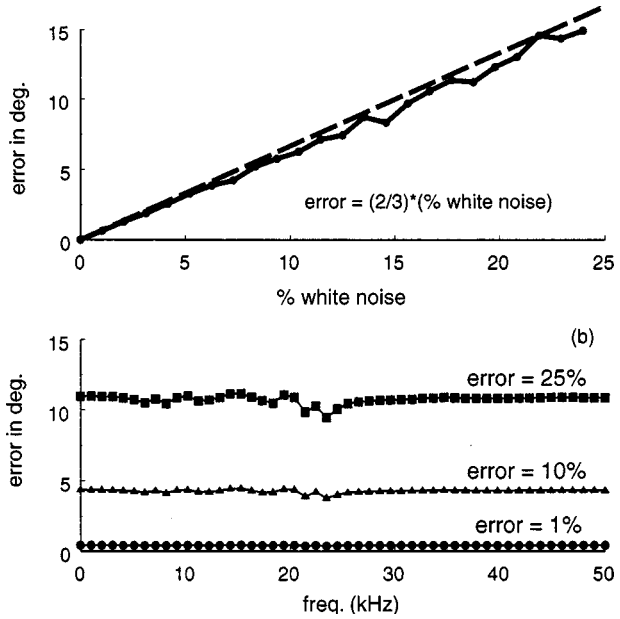

FIG. 7. Error in the phase calculation for (a) white noise compared to the dashed line prediction of Eq. (22) and (b) a second frequency component scanned over a range of frequencies and amplitudes.

A similar result holds when a second component is present in the signal. The signal detected is

$$f(t)=b(t)\cos[\varphi(t)]+c(t)\cos[\theta(t)], \tag{18}$$

where $b(t)\gg c(t)$. The application of the Hilbert transform determines the ''quadrature'' signal

$$g(t)=b(t)\sin[\varphi(t)]+c(t)\sin[\theta(t)]. \tag{19}$$

Calculating the amplitude using the condition $b(t)\gg c(t)$ for a Taylor's series expansion gives

$$\begin{aligned} a(t)&=\sqrt{f^2+g^2}=\sqrt{b^2+c^2+2bc\cos(\varphi-\theta)} \\ &=\sqrt{b^2\left(1+\frac{c^2}{b^2}+2\frac{c}{b}\cos(\varphi-\theta)\right)} \\ &\approx b\left(1+\frac{c}{b}\cos(\varphi-\theta)\right)\approx b+c, \end{aligned} \tag{20}$$

where the maximum value of 1 was used for the cosine term. Thus, the error in the amplitude is on the order of the magnitude of the second component.

The Hilbert transform also accurately calculates the phase in the presence of signal error. Calculating the phase error for the signal in Eq. (14) gives

$$\begin{aligned} \sigma_\varphi&=\sqrt{\left(\frac{\partial\varphi}{\partial f}\right)^2\sigma^2+\left(\frac{\partial\varphi}{\partial g}\right)^2\sigma^2} \\ &=\left[\left(\frac{-g}{f^2+g^2}\right)^2+\left(\frac{f}{f^2+g^2}\right)^2\right]^{1/2}\sigma=\frac{\sigma}{b}. \end{aligned} \tag{21}$$

Since the ratio σ/b is the fraction of error in the signal in radians, a useful formula is

$$\sigma_\varphi(\text{deg})=\frac{\%}{100}\frac{180}{\pi}\approx\frac{2}{3}\%, \tag{22}$$

where % stands for the percent of white noise in the signal. Figure 7 plots the effect of white noise and a second signal component on the phase calculation for the signal plotted in Fig. 1. In Fig. 7(a), white noise was added to the signal, and then the phase was calculated. This phase was compared to the phase of the base signal to determine the error. For white noise ranging from 0 to 25% of the signal amplitude, the phase error ranges linearly from 0 to 15°. The calculated error is very close to the error estimate from Eq. (22). Figure 7(b) illustrates the effect of a second signal component. The phase $\theta(t)$ of the second signal component of Eq. (19) was selected to be $2\pi\nu t$. The phase was calculated, and then compared to the phase of the base signal $b(t)\cos[\varphi(t)]$ at three different amplitude levels, ranging from 1% of the original signal up to 25%. This process was repeated by changing the frequency ν over the range from 0 to 50 kHz. The error in phase is independent of the frequency of the second component, and stays in the range of 0–15° for error amplitudes ranging from 0 to 25% of the original signal.

ACKNOWLEDGMENT

This research was supported by Department of Energy Grant No. DE-FG02-86ER53222.

[1] O. Sauter *et al.*, Phys. Plasmas **4**, 1654 (1997).
[2] R. Bracewell, *The Fourier Transform and Its Applications* (McGraw–Hill, New York, 1986), Chap. 12.
[3] L. Cohen, in *Time-Frequency Signal Analysis*, edited by B. Boashash (Wiley, New York, 1992), Chap. 1.
[4] L. Cohen, *Time-Frequency Analysis* (Prentice–Hall, New Jersey, 1995), Chap. 2.
[5] Y. Okunev, *Phase and Phase-Difference Modulation in Digital Communications* (Artech House, Boston, 1997), Appendix.
[6] A. Ghizzo, T. Réveillé, P. Bertrand, T. W. Johnston, J. Lebas, and M. Shoucri, J. Comput. Phys. **118**, 356 (1995).
[7] B. D. Fried and S. D. Conte, *The Plasma Dispersion Function* (Academic, New York, 1961), Chap. 1.
[8] M. E. Mauel, J. Bialek, C. Cates, H. Dahi, D. Maurer, D. Nadle, G. A. Navratil, M. Shilov, and E. Taylor, in *Plasma Physics and Controlled Nuclear Fusion Research 1998*, Proceedings of the 17th International Conference, Yokohama (International Atomic Energy Agency, Vienna in press).
[9] G. A. Navratil, C. Cates, M. E. Mauel, D. Maurer, D. Nadle, E. Taylor, Q. Xiao, W. A. Reass, and G. A. Wurden, Phys. Plasmas **5**, 1855 (1998).
[10] W. Morris, T. C. Hender, J. Hugill, P. S. Haynes, P. C. Johnson, B. Lloyd, D. C. Robinson, C. Silvester, S. Arshad, and G. M. Fishpool, Phys. Rev. Lett. **64**, 1254 (1990).
[11] A. I. Smolyakov, A. Hirose, E. Lazzaro, G. B. Re, and J. D. Callen, Phys. Plasmas **2**, 1581 (1995).
[12] J. Finn, Phys. Plasmas **5**, 3595 (1998).
[13] R. Fitzpatrick, Phys. Plasmas **2**, 825 (1995).
[14] P. C. de Vries, G. Waidmann, A. Krämer-Flecken, A. J. H. Donné, and F. C. Schüller, Plasma Phys. Controlled Fusion **39**, 439 (1997).
[15] P. VanMilligen, A. C. A. P. VanLammeren, N. J. Lopes Cardozo, F. C. Schüller, and M. Verreck, Nucl. Fusion **33**, 1119 (1993).
[16] O. Klüber, H. Zohm, H. Bruhns, J. Gernhardt, A. Kallenbach, and H. P. Zehrfeld, Nucl. Fusion **31**, 907 (1991).
[17] K. Oasa *et al.*, in *Plasma Physics and Controlled Nuclear Fusion Research 1994*, Proceedings of the 15th International Conference, Seville (International Atomic Energy Agency, Vienna, 1995), Vol. 2, p. 279.
[18] H. Gasquet and A. J. Wootton, Rev. Sci. Instrum. **68**, 1111 (1997).
[19] Registered trademark of Research Systems, Inc.
[20] Registered trademark of The Math Works, Inc.

[21] B. Boashash, Proc. IEEE **80**, 519 (1992).
[22] B. Boashash and G. Jones, in *Time-Frequency Signal Analysis*, edited by B. Boashash (Wiley, New York, 1992), Chap. 2.
[23] J. T. Scoville, R. J. LaHaye, A. G. Kellman, T. H. Osborne, R. D. Stambaugh, E. J. Strait, and T. S. Taylor, Nucl. Fusion **31**, 875 (1991).
[24] J. A. Snipes, D. J. Campbell, P. S. Haynes, T. C. Hender, M. Hugon, P. J. Lomas, N. J. Lopes Cardozo, M. F. F. Nave, and F. C. Schüller, Nucl. Fusion **28**, 1085 (1988).
[25] J. Mandel, *The Statistical Analysis of Experimental Data* (Dover, Mineola, NY, 1984), p. 74.